Inorg. Chem. **2005**, *44*, 1221–1229

Inorganic Chemistry

Article

X-ray Absorption Spectroscopic Investigation of the Spin-Transition Character in a Series of Single-Site Perturbed Iron(II) Complexes

Deanne Jackson Rudd,[†] Christian R. Goldsmith,[†] Adam P. Cole,[†] T. Daniel P. Stack,*,[†] Keith O. Hodgson,*,[†,‡] and Britt Hedman*,[‡]

Department of Chemistry, Stanford University, Stanford, California 94305, and Stanford Synchrotron Radiation Laboratory, Stanford University, Stanford, California 94309

Received September 2, 2004

Select ferrous spin-transition complexes with the pentadentate ligand 2,6-bis(bis(2-pyridyl)methoxymethane)pyridine (**PY5**) were examined using variable-temperature solution solid-state magnetic susceptibility, crystallography, X-ray absorption spectroscopy (XAS), and UV/vis absorption spectroscopy. Altering the single exogeneous ligand, X, of [Fe(**PY5**)(X)]$^{n+}$ is sufficient to change the spin-state of the complexes. When X is the weak-field ligand Cl^-, the resultant Fe complex is high-spin from 4 to 300 K, whereas the stronger-field ligand MeCN generates a low-spin complex over this temperature range. With intermediate-strength exogenous ligands (X = N_3^-, MeOH), the complexes undergo a spin-transition. [Fe(**PY5**)(N_3)]$^+$, as a crystalline solid, transitions gradually from a high-spin to a low-spin complex as the temperature is decreased, as evidenced by X-ray crystallography and solid-state magnetic susceptibility measurements. The spin-transition is also evident from changes in the pre-edge and EXAFS regions of the XAS Fe K-edge spectra on a ground crystalline sample. The spin-transition observed with [Fe(**PY5**)(MeOH)]$^{2+}$ appears abrupt by solid-state magnetic susceptibility measurements, but gradual by XAS analysis, differences attributed to sample preparation. This research highlights the strengths of XAS in determining the electronic and geometric structure of such spin-transition complexes and underscores the importance of identical sample preparation in the investigation of these physical properties.

Introduction

Mononuclear non-heme iron enzymes have been studied extensively due to their ability to function as oxidation catalysts in biosynthetic processes.[1−5] The study of the ferrous forms of these enzymes is often complicated by a lack of available spectroscopic techniques.[5] Structural data about the coordination sphere of the iron site(s) have been obtained traditionally through X-ray crystallography, yet an alternative way of accessing structural information is X-ray absorption spectroscopy (XAS). Study of the extended X-ray absorption fine structure (EXAFS) allows the identification of ligand atom types and the measurement of ligand−metal distances, while study of the pre-edge region provides complementary information about the coordination geometry and the electronic configuration of the metal center.[6]

Several heme proteins are known to undergo temperature-dependent spin-transitions, including myoglobin, hemoglobin, cytochrome *c* peroxidase, and prostaglandin H synthase.[7−11] At room temperature (RT), these proteins often exist as mixtures of high-spin (HS) and low-spin (LS) ferric complexes. The ratio of spin-states is dependent on the axially bound ligand(s) that also help to determine the spin-transition characteristics with changes in temperature. The reduced active site of superoxide reductase, a non-heme iron enzyme recently isolated from the hyperthermophilic archaeon *Pyrococcus furiosus*, cycles between a five-coordinate ferrous

---

* Author to whom correspondence should be addressed. E-mail: hedman@ssrl.slac.stanford.edu.

[†] Department of Chemistry.

[‡] Stanford Synchrotron Radiation Laboratory.

(1) Feig, A. L.; Lippard, S. J. *Chem. Rev.* **1994**, *94*, 759−805.

(2) Holm, R. H.; Kennepohl, P.; Solomon, E. I. *Chem. Rev.* **1996**, *96*, 2239−2314.

(3) Que, L., Jr. *J. Chem. Soc., Dalton Trans.* **1997**, 3933−3940.

(4) *Iron Metabolism. Inorganic Biochemistry and Regulatory Mechanisms*, 1st ed.; Ferreira, G. C., Moura, J. J. G., Franco, R., Eds.; Wiley: Weinheim, 1999.

(5) Solomon, E. I. *Inorg. Chem.* **2001**, *40*, 3656−3669.

(6) George, G. N.; Hedman, B.; Hodgson, K. O. *Nat. Struct. Biol.* **1998**, *5*, 645−647.

(7) Beetlestone, J.; George, P. *Biochemistry* **1963**, *3*, 707−714.

(8) Iizuka, T.; Kotani, M.; Yonetani, T. *Biochim. Biophys. Acta* **1968**, *167*, 257−267.

(9) Iizuka, T.; Kotani, M. *Biochim. Biophys. Acta* **1969**, *181*, 275−286.

(10) Iizuka, T.; Kotani, M. *Biochim. Biophys. Acta* **1969**, *194*, 351−363.

(11) Kulmacz, R. J.; Tsai, A.-L.; Palmer, G. *J. Biol. Chem.* **1987**, *262*, 10524−10531.

10.1021/ic048765l CCC: $30.25

structure and a six-coordinate ferric structure.[12] Both structures are HS under normal physiological conditions, but when cyanide is introduced to the oxidized enzyme at RT, the Fe^{III} center becomes LS.[13] This sensitivity to a single-site perturbation has been duplicated in a series of ferrous and ferric complexes with the pentadentate ligand 2,6-bis(bis(2-pyridyl)methoxymethane)pyridine (**PY5**).[14] The **PY5** ligand, itself, binds metals consistently in a square-pyramidal geometry, leaving a sixth site open for an exogenous monodentate ligand.[14,15] This ligation attribute has allowed the structural and functional modeling of the iron- and manganese-containing lipoxygenases.[16,17]

The sensitivity of the EXAFS region in an XAS spectrum to small changes in metal−ligand distances is useful in studying the geometric changes associated with a spin-transition, as the anticipated ligand contraction from a HS configuration to a LS configuration in an octahedral Fe^{III} or Fe^{II} complex is typically ∼0.1 or 0.2 Å, respectively.[18,19] Further, the electronic changes expected as a result of the spin-transition should be reflected in the pre-edge region of the Fe K-edge.[20] Combined, these data provide structural insights not always obtainable from susceptibility data.

Here, we present the systematic XAS study of select ferrous **PY5** complexes. The HS [Fe(**PY5**)(Cl)](OTf) (OTf $= CF_3SO_3^-$), the LS [Fe(**PY5**)(MeCN)]$(OTf)_2$, and the spin-transition complexes, [Fe(**PY5**)(N_3)](OTf) and [Fe(**PY5**)(MeOH)]$(OTf)_2$, have been selected for this study due to their contrasting spin-state behaviors upon cooling. Comparisons are also made to LS [Fe(**PY5**)(CN)](OTf) and [Fe(**PY5**)(pyridine)]$(OTf)_2$. The spin-crossover is studied in the solid state primarily by XAS to assess the electronic and structural changes. This series of complexes provides an extensive systematic study of a single-site coordination sphere perturbation on the spin-state of the metal center.[21,22]

Experimental Section

A. Syntheses. All starting materials were purchased from Aldrich and used without further purification unless noted otherwise. All solvents and gases were of analytical grade and were purified by literature methods.[23] MeOH was distilled from $Mg(OMe)_2$ under N_2 and stored in darkness over 4 Å molecular sieves. Anhydrous diethyl ether (ether) was stored over 4 Å molecular sieves. When air-free solutions were necessary, the solvents were degassed prior to use. The iron complexes for crystallographic analysis were synthesized and handled under a N_2 inert atmosphere using a MBraun Labmaster 130 glovebox or standard Schlenk-line techniques. The synthesis and characterization of 2,6-bis(bis(2-pyridyl)methoxymethane)pyridine (**PY5**), [Fe(**PY5**)(MeOH)]$(OTf)_2$, [Fe(**PY5**)(MeCN)]$(OTf)_2$, [Fe(**PY5**)(N_3)](OTf), [Fe(**PY5**)(pyridine)]$(OTf)_2$, [Fe(**PY5**)(CN)](OTf), [Fe(**PY5**)(Cl)](OTf), and [Fe(**PY5**)(Cl)](Cl) have been described previously.[14,16,24]

B. Instrumentation. ^{1}H NMR spectra were recorded on a Varian Gemini-400 (400 MHz) or a Varian Inova-500 (500 MHz) NMR spectrometer, and chemical shifts are reported in ppm downfield from an internal TMS reference. Electronic spectra were measured on a Polytec X-dap fiber optics UV/vis diode array spectrophotometer or a Cary 50 Bio UV−visible spectrophotometer. Solution magnetic moments were determined by the Evans method in d_3-MeOD.[25,26] Solid-state magnetic susceptibility measurements were collected using a Quantum Design MPMS2 SQUID magnetometer.

C. Magnetic Susceptibility. To correlate directly to the mole fractions of each electronic configuration, the molar susceptibilities per ferrous site, $\chi_M T$, are presented; a $\chi_M T$ value near 3.0 cm^3 K mol^{-1} corresponds to a pure-HS ferrous complex. Least-squares fitting of the susceptibility data was performed using an Excel spreadsheet with all data points equally weighted. For solution measurements in d_3-MeOD, the solvent contraction was calculated assuming that the density change of h_3-MeOH with temperature is identical to that for d_3-MeOD and using a density of 0.888 g cm^{-3} for d_3-MeOD at 293 K. The least-squares fits allowed the enthalpy, entropy, and $\chi_M T_{HS}$, the value for a pure-HS ferrous complex, to vary. The paramagnetic contribution of the LS component was assumed to be zero.

D. X-ray Crystallography. The two X-ray data sets for [Fe(**PY5**)(N_3)](OTf) were measured at 240 and 135 K with different crystals. In each case, a suitably sized crystal was mounted in paratone oil on a glass fiber and placed in a cold stream of N_2 on a Siemens CCD diffractometer with graphite monochromated Mo Kα radiation ($\lambda = 0.71073$ Å). The data were corrected for Lorentz and polarization effects. The structures were solved by direct methods and expanded using Fourier techniques. All non-hydrogen atoms were refined anisotropically, unless otherwise noted. Hydrogen atoms were located by difference Fourier maps, but included at idealized position from their parent atoms for the final refinement. Isotropic thermal parameters 1.2 times the parent atoms were assumed. Neutral atom scattering factors were taken from Cromer and Waber.[27] Anomalous dispersion effects were included in F_{calc};[28] the values for $\Delta f'$ and $\Delta f''$ were those of Creagh and McAuley.[29] The values for the mass attenuation coefficients are those of Creagh

---

(12) Yeh, A. P.; Hu, Y.; Jenney, F. E., Jr.; Adams, M. W. W.; Rees, D. C. *Biochemistry* **2000**, *39*, 2499−2508.

(13) Clay, M. D.; Jenney, F. E., Jr.; Hagedoorn, P. L.; George, G. N.; Adams, M. W. W.; Johnson, M. K. *J. Am. Chem. Soc.* **2002**, *124*, 788−805.

(14) Goldsmith, C. R.; Jonas, R. T.; Cole, A. P.; Stack, T. D. P. *Inorg. Chem.* **2002**, *41*, 4642−4652.

(15) Gebbink, R. J. M. K.; Jonas, R. T.; Goldsmith, C. R.; Stack, T. D. P. *Inorg. Chem.* **2002**, *41*, 4633−4641.

(16) Goldsmith, C. R.; Jonas, R. T.; Stack, T. D. P. *J. Am. Chem. Soc.* **2002**, *124*, 83−96.

(17) Goldsmith, C. R.; Cole, A. P.; Stack, T. D. P., manuscript submitted.

(18) Hannay, C.; Hubin-Franskin, M.-J.; Grandjean, F.; Briois, V.; Itie, J.-P.; Polian, A.; Trofimenko, S.; Long, G. J. *Inorg. Chem.* **1997**, *36*, 5580−5588.

(19) *Spin Crossover in Transition Metal Compounds I*; Gütlich, P., Goodwin, H. A., Eds.; Springer-Verlag: Berlin, 2004; Vol. 233.

(20) Westre, T. E.; Kennepohl, P.; DeWitt, J. G.; Hedman, B.; Hodgson, K. O.; Solomon, E. I. *J. Am. Chem. Soc.* **1997**, *119*, 6297−6314.

(21) Toftlund, H.; McGarvey, J. J. Iron(II) Spin Crossover Systems with Multidentate Ligands. In *Spin Crossover in Transition Metal Compounds I*; Gütlich, P., Goodwin, H. A., Eds.; Springer-Verlag: Berlin, 2004; Vol. 233, pp 151−166.

(22) Cairns, C.; Nelson, S. M.; Drew, M. G. B. *J. Chem. Soc., Dalton Trans.* **1981**, 1965−1972.

(23) Perrin, D. D.; Armarego, W. L. F. *Purification of Laboratory Chemicals*, 1st ed.; Pergamon Press: New York, 1988.

(24) Jonas, R. T.; Stack, T. D. P. *J. Am. Chem. Soc.* **1997**, *119*, 8566−8567.

(25) Evans, D. F. J. *J. Chem. Soc.* **1959**, 2003−2005.

(26) Sur, S. K. *J. Magn. Reson.* **1989**, *82*, 169−173.

(27) Cromer, D. T.; Waber, J. T. *International Tables for X-ray Crystallography*; Kynoch: Birmingham, 1974.

(28) Ibers, J. A.; Hamilton, W. C. *Acta Crystallogr.* **1964**, *17*, 781−782.

(29) Creagh, D. C.; McAuley, W. J. In *International Tables for Crystallography*; Wilson, A. J. C., Ed.; Kluwer Academic Publishers: Boston, MA, 1992; Vol. C, pp 219−222, Table 4.2.6.8.

and Hubbell.[30] All calculations were performed using the teXsan crystallographic software package of Molecular Structure Corp.; refinements were performed using SHELXL-97. ORTEP representations with a detailed numbering scheme and complete tables of positional parameters, bond lengths, bond angles, and anisotropic thermal factors are available.[31]

E. X-ray Absorption Spectroscopic Measurements. 1. Sample Preparation. Approximately 25 mg of each crystalline sample was ground on the benchtop in a matrix of ~25 mg of boron nitride to create a homogeneous sample and to eliminate the phenomenon of self-absorption effects during data collection. The resultant fine powder was then pressed into a 2 mm Al spacer with Mylar tape windows and sealed in an Al holder.

2. Data Collection and Reduction. The X-ray absorption spectra for the $[Fe^{II}(\mathbf{PY5})(\mathbf{X})]^{n+}$ samples were measured at the Stanford Synchrotron Radiation Laboratory (SSRL) on unfocused 8-pole wiggler beam line 7-3 (X = MeCN, MeOH, N_3^-) and on focused 16-pole wiggler beam line 9-3 (X = MeCN, CN^-, pyridine, MeOH, Cl^-) with the ring operating at 3 GeV, 50−100 mA. A Si(220) monochromator was utilized for energy selection at the Fe K-edge. The monochromator was detuned 50% at 7987 eV to minimize higher harmonic components in the X-ray beam on beam line 7-3. A collimating harmonic rejection mirror was present on beam line 9-3, resulting in a slightly higher energy resolution on beam line 9-3 as compared to beam line 7-3. Data were measured to $k = 15$ Å^{-1} in transmission mode, and internal energy calibration was performed by simultaneous measurement of the absorption of an Fe foil placed between two ionization chambers located after the sample. The first inflection point of the foil was assigned to 7111.2 eV. Scans were taken on all samples at RT and 10 K. All non-RT data were collected using an Oxford Instruments CF1208 continuous flow liquid He cryostat. For spectra measured at 10 K, the cryostat was maintained at this temperature and the sample was introduced into the cryostat after being flash frozen in liquid N_2. Variable-temperature studies of $[Fe(\mathbf{PY5})(MeOH)]^{2+}$ were initiated by placing the unfrozen sample into the cryostat stabilized at 150 K. Two full EXAFS scans (to $k = 15$ Å^{-1}) were taken at 150 K before the temperature was lowered at ~1 K/min to 120 K. Two full EXAFS scans were measured at 120 K. The sample was then allowed to cool at ~1 K/min from 120 to 40 K, with short scans to $k = 5$ Å^{-1} being started at 90, 80, 70, 60, and 50 K. The cryostat temperature was stabilized at 40 K, and full EXAFS scans ($k = 15$ Å^{-1}) were measured at 40 K and subsequently at 10 K. The total cooling and scanning process took ~8 h.

The averaged data were processed by fitting a first-order polynomial to the pre-edge region and subtracting this background from the entire spectrum. A three-region spline of orders 2, 3, and 3 was used to model the smooth background above the edge. Normalization of the data was achieved by subtracting the spline and normalizing the edge jump to 1.0 in the post-edge region between 7300 and 7800 eV. The resultant EXAFS was k^3-weighted to enhance the impact of high-k data. In some cases, the data were truncated at $k = 12$ Å^{-1} due to interference from a monochromator glitch in this region or the signal-to-noise ratio.

3. EXAFS Data Analysis. Theoretical EXAFS signals $\chi(k)$ were calculated using FEFF (version 7.02)[32−35] and fit to the data using EXAFSPAK.[36] The experimental energy threshold, E_0 (the point at which $k = 0$), was chosen as 7130 eV and was allowed to vary by a common amount (ΔE_0) for all components within a given fit. The structural parameters that were varied during the refinements include the bond distance (R) and the bond variance (σ^2). The σ^2 parameter is related to the Debye−Waller factor, which is a measure of thermal vibration and static disorder of the absorbers and scatterers. Coordination numbers were systematically varied during the course of the analysis, but were not allowed to vary within a given fit. More distant second-shell single and multiple-scattering waves were fit with carbon components from FEFF. Debye−Waller factors were allowed to float in all fits, while coordination numbers were fixed to chemically reasonable values. Multiple-scattering contributions were not linked to the corresponding single-scattering contributions, but were allowed to float freely in all fits.

4. Pre-Edge Analysis. The energies and intensities of the pre-edge transitions were determined by least-squares fits to the data using EDG_FIT.[36] Pseudo-Voigt line shapes (sums of Lorentzian and Gaussian functions) were used to model the pre-edge features. The amplitude, energy position, and full width at half-maximum (fwhm) were varied for each peak during the fitting procedure. A wide transition was used as a background and was considered acceptable as long as it remained lower in intensity than the white line of the edge. The data and the second derivative of the data were fit simultaneously, and both were required to be well fit within the noise of the data for the fit to be acceptable. All data were fit over three energy ranges (7108−7116, 7108−7117, 7108−7118 eV), and three fits were attempted for each range, for a total of nine fits for each complex. The first fit allowed the background and transition parameters (amplitude, position, and fwhm) to float freely to the best fit. The two subsequent fits fixed the fwhm of the background peak to a value ±0.5 from the original value and allowed all other parameters to float. The value reported for the energy position and intensity (calculated as amplitude multiplied by fwhm) of each transition is an average of that value for all successful fits, and the error is the standard deviation for that value over all successful fits, as described in detail previously.[20]

Results

A. Solution Measurements. The magnetic susceptibilities of $[Fe(\mathbf{PY5})(X)]^{n+}$ ($\mathbf{X}$ = MeCN, pyridine, CN^-, Cl^-, N_3^-, MeOH) were determined in d_3-MeOD solution by the Evans method.[25,26] The $[Fe(\mathbf{PY5})(X)]^{n+}$ complexes with strong field, π-accepting ligands (X = MeCN, pyridine, CN^-) are effectively diamagnetic at 293 K as evidenced by their sharp ^{1}H NMR signals in the 1−14 ppm range and negligible susceptibilities. The remaining complexes (X = Cl^-, N_3^-, MeOH) exist predominantly in a HS electronic configuration under similar conditions.[14,16] $[Fe(\mathbf{PY5})(Cl)](Cl)$ has a $\chi_M T$ value of 2.8(2) cm^3 K mol^{-1} [15] at 293 K that does not change significantly at 200 K ($\chi_M T$ = 2.6(2) cm^3 K mol^{-1}),[15] consistent with a HS complex.

In contrast, the $\chi_M T$ values of $[Fe(\mathbf{PY5})(N_3)]^+$ and $[Fe(\mathbf{PY5})(MeOH)]^{2+}$ decrease significantly with temperature in d_3-MeOD solution. For $[Fe(\mathbf{PY5})(N_3)]^+$, the $\chi_M T$ value of

---

[30] Creagh, D. C.; Hubbell, J. H. In *International Tables of Crystallography*; Wilson, A. J. C., Ed.; Kluwer Academic Publishers: Boston, MA, 1992; Vol. C, pp 200−206, Table 4.2.4.3.

[31] See Supporting Information.

[32] Rehr, J. J.; Mustre de Leon, J.; Zabinsky, S. I.; Albers, R. C. *J. Am. Chem. Soc.* **1991**, *113*, 5135−5140.

[33] Mustre de Leon, J.; Rehr, J. J.; Zabinsky, S. I.; Albers, R. C. *Phys. Rev. B* **1991**, *44*, 4146−4156.

[34] Zabinsky, S. I.; Rehr, J. J.; Ankudinov, A.; Albers, R. C.; Eller, M. J. *Phys. Rev. B* **1995**, *52*, 2995−3009.

[35] Rehr, J. J.; Albers, R. C. *Rev. Mod. Phys.* **2000**, *72*, 621−654.

[36] George, G. N. EXAFSPAK & EDG_FIT, 2000, Stanford Synchrotron Radiation Laboratory, Stanford Linear Accelerator Center, Stanford University, Stanford, CA 94309.

2.8(2) cm^3 K mol^{-1} at 293 K is reduced to 1.1(2) cm^3 K mol^{-1} at 203 K (MeOH freezes at 185 K). Assuming a simple LS to HS equilibrium model, a least-squares fit of the susceptibility data in the form of a $\chi_M T$ versus temperature plot gives $\Delta H° = +6.8$ kcal mol^{-1}, $\Delta S° = +33$ cal K^{-1} mol^{-1}, and $\chi_M T_{HS} = 2.67$ cm^3 K mol^{-1}, the $\chi_M T$ value for the pure HS complex (Figure S1). This model predicts an inversion temperature of 207 K, the temperature at which the mole fraction of the LS and HS sites are equal. Additionally, the model predicts that greater than 99% of the sites are HS at 293 K which reduces to 40% at 203 K. This transition is also evident from variable-temperature solution UV/vis spectroscopy, as the ligand-to-metal charge-transfer (LMCT) bands in the UV/vis spectrum of [Fe(**PY5**)(N$_3$)]$^+$ shift and increase in intensity with cooling of the solution (Figure S2). Variable-temperature susceptibility and optical spectroscopy measurements of [Fe(**PY5**)(MeOH)]$^{2+}$ reveal similar behavior in MeOH, yet the magnitudes of the changes are not as large (Figure S3). $\chi_M T$ values of 3.5(2) and 2.4(2) cm^3 K mol^{-1} at 293 and 203 K, respectively, suggest that 68% of the sites remain in the HS configuration at the lower temperature. A least-squares fit of the $\chi_M T$ versus temperature plot to an equilibrium model gives $\Delta H° = +4.3$ kcal mol^{-1}, $\Delta S° = +22$ cal K^{-1} mol^{-1}, and $\chi_M T_{HS} = 3.6$ cm^3 K mol^{-1} (Figure S4) with an inversion temperature of 192 K. With a lesser conversion to the LS state at 203 K as compared to [Fe(**PY5**)(N$_3$)]$^+$, the changes in the optical spectrum of [Fe(**PY5**)(MeOH)]$^{2+}$ from 293 K are also smaller.[31]

B. Solid-State Magnetic Susceptibility. The solid-state magnetic susceptibilities of [Fe(**PY5**)(X)]$^{n+}$ (X = Cl$^-$, N$_3^-$, MeOH) were determined with a SQUID magnetometer between 5 and 300 K. A ground crystalline solid of [Fe(**PY5**)(Cl)](OTf) exhibits a $\chi_M T$ value of 3.3 cm^3 K mol^{-1} at 295 K that remains unchanged effectively upon cooling to 5 K, a behavior fully consistent with a HS ferrous complex (Figure S5). This contrasts with the behavior of the solid crystalline sample of [Fe(**PY5**)(N$_3$)](OTf)·2H$_2$O that exhibits a $\chi_M T$ value of 3.3 cm^3 K mol^{-1} at 295 K that gradually decreases to 0.5 cm^3 K mol^{-1} at 70 K and plateaus until 10 K (Figure 1a). This transition displays a minor hysteresis in the higher temperature range. Assuming a simple ferrous spin-crossover complex in which the residual paramagnetic component below 50 K is associated with trapped HS sites, the $\chi_M T$ value of ~0.5 cm^3 K mol^{-1} corresponds to ~15% of the bulk sample.[37] Assuming that this HS fraction persists at all temperatures, the 295−50 K data can be fitted to a simple LS to HS solution model assuming no cooperativity. The least-squares fit gives $\Delta H° = +1.51$ kcal mol^{-1}, $\Delta S° = +9.6$ cal K^{-1} mol^{-1}, and a $\chi_M T_{HS} = 3.68$ cm^3 K mol^{-1}.[38] These fitted parameters yield $T_{1/2} = 156$ K (Figure S6) and predict that for the entire sample at 295, 240, and 135 K, 91%, 87%, and 40% of the sites are HS, respectively. Slight grinding of crystalline [Fe(**PY5**)(N$_3$)](OTf)·2H$_2$O leads to dramatically different magnetic behavior; the $\chi_M T$ value over the entire temperature range does not change appreciably from a value of 3.3 cm^3 K mol^{-1} (Figure 1a).

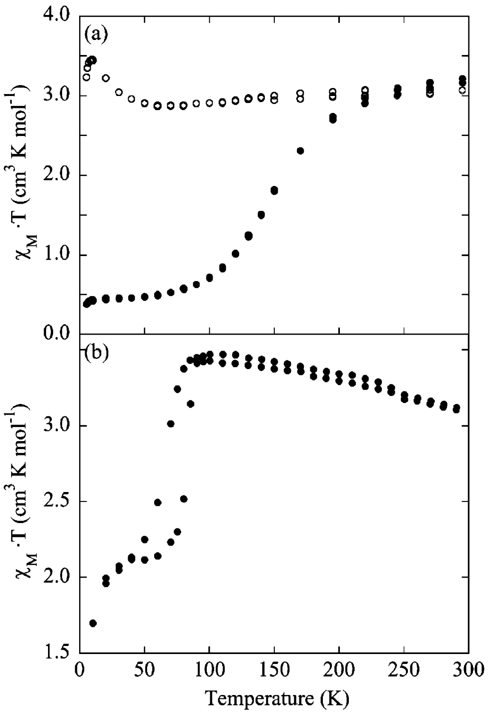

Figure 1. (a) Solid-state SQUID data for (a) crystalline (●) and ground (○) [Fe(**PY5**)(N$_3$)]$^+$ and (b) crystalline [Fe(**PY5**)(MeOH)]$^{2+}$. Both samples were gradually cooled (top data in (b)) from 300 to 4 K and then warmed (bottom data in (b)) to 300 K.

Scheme 1

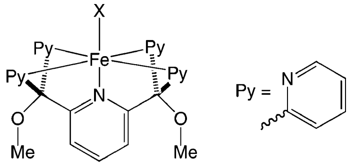

[Fe(**PY5**)(MeOH)]$^{2+}$ undergoes an abrupt transition to a lower spin-state at ~90 K and displays a significant hysteresis as it returns to 300 K (Figure 1b). The magnitude of the spin-state change and hysteresis are very dependent on sample preparation. Grinding of the crystalline sample seemingly decreases the proportion that undergoes a spin-transition, and a complete transition to a LS complex is never observed. Thus, as with [Fe(**PY5**)(N$_3$)]$^+$, the magnitude of the spin change in [Fe(**PY5**)(MeOH)]$^{2+}$ varies dramatically with sample preparation.

C. Solid-State Structures. The X-ray crystal structures of [Fe(**PY5**)(MeCN)]$^{2+}$,[39] [Fe(**PY5**)(Cl)]$^+$,[14,15] and [Fe(**PY5**)(MeOH)]$^{2+}$,[16,24] as previously reported, have the general structure of the cation that is graphically depicted in Scheme 1. Important metrical parameters for these structures are summarized in Table 1. [Fe(**PY5**)(N$_3$)]$^+$ crystallized as a stable orange solid with an asymmetric unit containing the cation [Fe(**PY5**)(N$_3$)]$^+$, two water molecules, and a triflate

---

(37) Singh, S.; Mishra, V.; Mukherjee, J.; Seethalekshmi, N.; Mukherjee, R. *Dalton Trans.* **2003**, 3392−3397.

(38) van Koningsbruggen, P. J.; Garcia, Y.; Kahn, O.; Fournes, L.; Kooijman, H.; Spek, A. L.; Haasnoot, J. G.; Moscovici, J.; Provost, K.; Michalowicz, A.; Renz, F.; Gütlich, P. *Inorg. Chem.* **2000**, *39*, 1891−1900.

(39) de Vries, M. E.; La Crois, R. M.; Roelfes, G.; Kooijman, H.; Spek, A. L.; Hage, R.; Feringa, B. L. *Chem. Commun.* **1997**, 1549−1550.

Table 1. Selected Bond Lengths in [Fe(**PY5**)(X)]$^{n+}$ Complexes (Å) As Determined by X-ray Crystallography[a]

X	temp (K)	Fe−X	Fe−N$_1$	Fe−N$_2$	Fe−N$_3$	Fe−N$_4$	Fe−N$_5$	Fe−X$_{ave}$
MeCN[39]	150	1.952(8)	1.927(8)	2.078(8)	2.076(8)	1.995(9)	1.957(8)	1.998
CN$^-$ [14]	203	1.925(3)	1.980(2)	2.000(2)	2.068(2)	2.043(2)	2.003(2)	2.003
pyridine[14]	203	1.992(8)	1.987(8)	2.012(8)	1.996(8)	2.060(8)	1.999(8)	2.008
Cl$^-$ [14]	203	2.311(2)	2.198(5)	2.182(5)	2.272(5)	2.252(4)	2.173(5)	2.215[b]
MeOH[24]	203	2.040(3)	2.097(3)	2.152(3)	2.203(3)	2.217(3)	2.141(3)	2.142
N$_3$$^-$	240	2.061(4)	2.145(3)	2.167(3)	2.229(3)	2.215(3)	2.157(3)	2.162
N$_3$$^-$	135	2.020(5)	2.002(4)	2.045(4)	2.101(4)	2.082(4)	2.024(2)	2.046

[a] Estimated standard deviations in the least significant figure are given in parentheses. [b] Average does not include Fe−Cl distance.

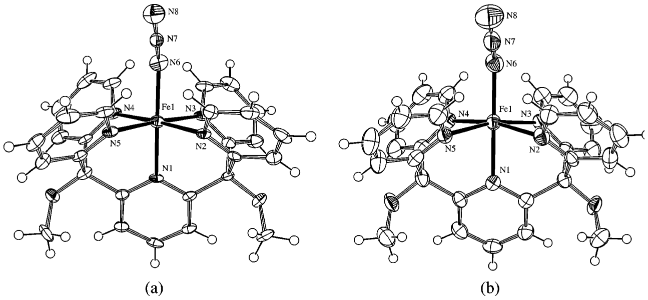

(a) (b)

Figure 2. ORTEP representations of [Fe(**PY5**)(N$_3$)]$^+$ at (a) 135 K and (b) 240 K. Ellipsoids are drawn at the 50% probability level.

Table 2. Crystal Data and Data Collection Details of [Fe(**PY5**)(N$_3$)](OTf) at 135 and 240 K[a,b]

	135 K	240 K
formula	$C_{30}H_{29}N_5O_7F_3SFe$	$C_{30}H_{29}N_5O_7F_3SFe$
fw (g mol^{-1})	758.52	758.52
space group	$P2_1/n$ (No. 14)	$P2_1/n$ (No. 14)
cryst syst	monoclinic	monoclinic
a (Å)	12.6873(4)	12.8464(4)
b (Å)	14.2689(2)	14.6178(2)
c (Å)	17.8825(7)	17.9208(7)
β (deg)	103.341(2)	103.873(2)
V (Å^3)	3150.0(2)	3267.1(2)
Z	4	4
μ_{calc} (cm^{-1})	6.25	6.03
F_{000}	1560	1560
ρ_{calc} (g cm^{-3})	1.599	1.542
cryst size (mm)	0.14 × 0.18 × 0.21	0.21 × 0.20 × 0.17
2θ range (deg)	$4.00° < 2\theta < 46.50°$	$4.00° < 2\theta < 43.92°$
reflns collected	12 559	11 651
unique reflns	4506 ($R_{int} = 0.089$)	3984 ($R_{int} = 0.070$)
reflns with ($F_o^2 > 4\sigma(F_o^2)$)	2273	2555
number of params	363	363
reflns/params ratio	12.41	10.98
R (R_w)[c]	0.057 (0.135)	0.050 (0.121)
final diff. ρ_{max}[d] (e$^-$/Å^3)	0.46	0.29

[a] All data collected with graphite monochromated Mo Kα radiation (λ = 0.71073 Å) using ω scans. [b] A different crystal was used for each data set. [c] The unweighted and weighted agreement factors in the least-squares refinements were: $R = \sum||F_o| - |F_c||/\sum|F_o|$; $R_w = [\sum(w(F_o^2 - F_c^2)^2)/\sum w(F_o^2)^2]^{1/2}$, where $w = 1/[\sigma^2(F_o^2) + (0.0815P)^2]$, where $P = (F_o^2 + 2F_c^2)/3$ for $F_o^2 >= 0$; $2F_c^2/3$ for $F_o^2 < 0$. [d] Maximum negative and positive difference peaks.

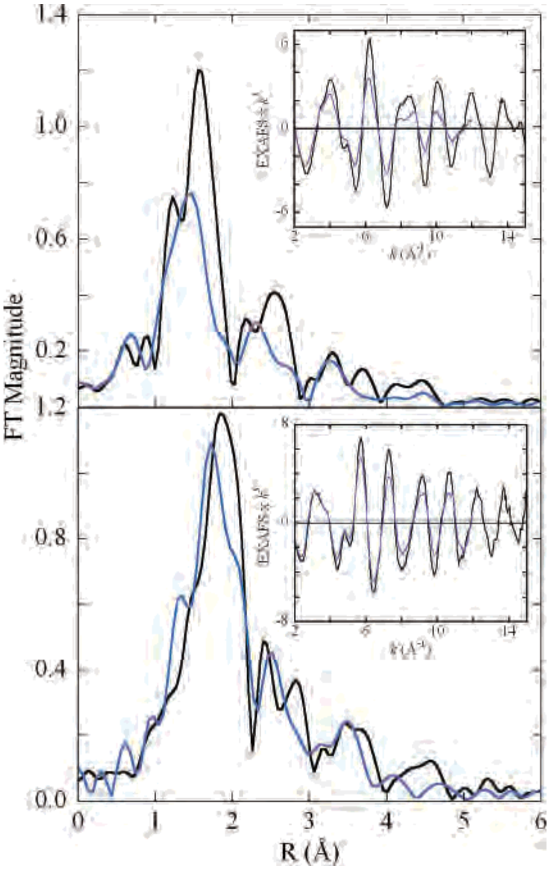

Figure 3. Non-phase-shift corrected Fourier transforms (and EXAFS data, inset) for (a) [Fe(**PY5**)(MeCN)]$^{2+}$ and (b) [Fe(**PY5**)(Cl)]$^+$ at RT (blue) and 10 K (black). Note that the peaks and troughs in the EXAFS data are in the same location regardless of temperature, but the amplitude of the wave is decreased in the RT data sets.

counteranion (Figure 2, Table 2). The metrical parameters are dependent on the temperature at which the crystallographic data were acquired (Table 1). At 135 K (Figure 2a), the average of the six Fe−N distances is 2.05 Å and the iron center is displaced +0.08 Å toward the azide from the plane defined by N$_{2-5}$. Both of these metrics are most consistent with a LS [Fe(**PY5**)(X)]$^{n+}$ complex.[14] At 240 K (Figure 2b), the average Fe−N distance lengthens to 2.16 Å and the Fe center is further displaced above the N$_{2-5}$ plane (0.22 Å) as compared to the 135 K structure. These metrical parameters are most consistent with a HS Fe^{II} center. Interestingly, the Fe−N$_6$ distance to the azide ligand does not lengthen dramatically, elongating from 2.02 Å (135 K) to 2.06 Å (240 K).

D. X-ray Absorption Spectroscopy. 1. EXAFS Analysis. To better understand the geometric changes that occur in [Fe(**PY5**)(N$_3$)]$^+$ and [Fe(**PY5**)(MeOH)]$^{2+}$, EXAFS data were collected for [Fe(**PY5**)(MeCN)]$^{2+}$ and [Fe(**PY5**)(Cl)]$^+$ that have been shown by the other methods, as described above, to maintain their spin-state at all examined temperatures. Figure 3a shows the non-phase-shifted Fourier transform (FT) and EXAFS data (inset) for [Fe(**PY5**)(MeCN)]$^{2+}$ at RT and at 10 K, and Figure 3b shows those for [Fe(**PY5**)(Cl)]$^+$. The RT data for both complexes show the effect of thermal disorder on the EXAFS signal. As the temperature is increased, the EXAFS signal becomes damped due to the increased thermal vibrations of the atoms in the molecule.

Table 3. EXAFS Fit Results for $[Fe(\mathbf{PY5})(MeCN)]^{2+}$ and $[Fe(\mathbf{PY5})(Cl)]^{+}$ at RT and 10 K[a]

	R (Å)	σ^2 (Å^2)	ΔE_0	F[b]
	$[Fe(\mathbf{PY5})(MeCN)]^{2+}$ RT			
6 N	1.99	0.0109	−7.57	0.086
13 C_2	2.93	0.0127		
11 N−C_2	3.13	0.0164		
10 N−C_3	4.36	0.0310		
5 N−C_4	4.77	0.0114		
	$[Fe(\mathbf{PY5})(MeCN)]^{2+}$ 10 K			
6 N	1.99	0.0044	−6.76	0.23
13 C_2	2.93	0.0072		
11 N−C_2	3.13	0.0110		
10 N−C_3	4.32	0.0155		
5 N−C_4	4.79	0.0052		
	$[Fe(\mathbf{PY5})(Cl)]^{+}$ RT			
5 N	2.17	0.0099	−10.52	0.13
1 Cl	2.32	0.0020		
12 C_2	3.09	0.0107		
10 N−C_2	3.41	0.0112		
10 N−C_3	4.48	0.0099		
5 N−C_4	5.02	0.0104		
	$[Fe(\mathbf{PY5})(Cl)]^{+}$ 10 K			
5 N	2.18	0.0052	−9.15	0.24
1 Cl	2.34	0.0010		
12 C_2	3.10	0.0071		
10 N−C_2	3.42	0.0098		
10 N−C_3	4.49	0.0061		
5 N−C_4	4.99	0.0058		

[a] Errors are estimated to be 0.01−0.03 Å for distances and 25% for coordination numbers. [b] Error (F) is defined as $F = \sum[[(\chi_{obsd} - \chi_{calcd})^2 k^6]/n]$, where n is the number of data points.

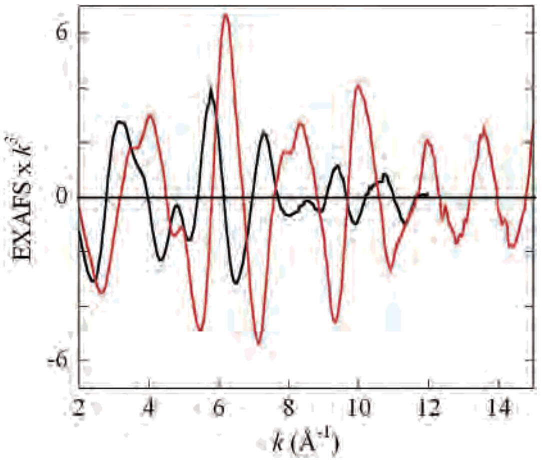

Figure 4. EXAFS data at RT (black) and 10 K (red) for $[Fe(\mathbf{PY5})(N_3)]^{+}$, indicating the geometric changes in the Fe site as the complex transitions from a HS to a LS configuration.

The locations of the peaks and troughs of the EXAFS wave in the RT data, however, match those of the 10 K data well, despite the reduction in overall amplitude. Fit results for each data set give virtually identical iron−ligand distances for each complex at the two temperatures (Figure S7, Table 3). The σ^2 values for the RT data are higher than those at 10 K, as expected. It should be noted that the averaged structural values obtained by EXAFS analysis correlate well in both cases to those found by X-ray diffraction (Table 1).

Susceptibility measurements suggest that $[Fe(\mathbf{PY5})(N_3)]^{+}$ undergoes a HS to LS transition with cooling. Differences in the EXAFS spectra at RT and 10 K cannot be attributed to the decrease in thermal disorder with cooling (Figure 4).

Table 4. EXAFS Fit Results for $[Fe(\mathbf{PY5})(N_3)]^{+}$ at RT and at 10 K[a]

	R (Å)	σ^2 (Å^2)	ΔE_0	F[b]
		RT		
2 N	2.04	0.0038	−9.05	0.035
4 N	2.19	0.0043		
13 C_2	3.08	0.0111		
10 N−C_2	3.37	0.0215		
2 N−N	3.94	0.0096		
10 N−C_3	4.48	0.0206		
5 N−C_4	5.04	0.0131		
		10 K		
6 N	2.00	0.0045	−7.70	0.24
13 C_2	2.95	0.0072		
10 N−C_2	3.05	0.0183		
2 N−N	3.78	0.0050		
10 N−C_3	4.40	0.0206		
5 N−C_4	4.80	0.0051		

[a] Errors are estimated to be 0.01−0.03 Å for distances and 25% for coordination numbers. [b] Error (F) is defined as $F = \sum[[(\chi_{obsd} - \chi_{calcd})^2 k^6]/n]$, where n is the number of data points.

Fits to the RT EXAFS data (Figure S7, Table 4) find 2 N scatterers at 2.04 Å and 4 N scatterers at 2.19 Å (Fe−N_{ave} = 2.14 Å), similar to the Fe−N_{ave} of 2.16 Å observed in the X-ray structure determined at 240 K (Table 1). The sample measured at 10 K is best fit with 6 N scatterers at 2.00 Å, which correlates best to the 135 K X-ray structure. The 0.14 Å decrease in the Fe−N_{ave} distance is of the magnitude expected for a change on going from a HS to LS ferrous complex.[19]

EXAFS scans of $[Fe(\mathbf{PY5})(MeOH)]^{2+}$ at RT, 150, 120, 40, and 10 K show clear isosbestic behavior, suggesting variable mole fractions of two species in each scan (Figure 5). Assuming a pure HS and pure LS sample at RT and 10 K, respectively, linear combinations of spectra at these temperatures can be used to simulate the data at intermediate temperatures. Although the amplitude of the EXAFS wave is not well simulated due to the nonlinear differences in thermal disorder at different temperatures,[40,41] the position of the peaks and troughs is informative. A linear combination estimates that, at 150 K, ∼30% of the sample is LS and, at 120 K, ∼70% of the sample is LS (Figure S8). These results are consistent with those from solution magnetic susceptibility that found ∼70% residual HS character in the sample at 203 K. Fits to the RT and 10 K data (Figure S7, Table 5) reveal the expected metric changes. The RT fit includes 6 N/O scatterers at 2.13 Å, consistent with a HS ferrous complex, while the first shell of the 10 K data fit to a distance of 2.00 Å for 6 N/O scatterers, consistent with a LS ferrous complex. Corresponding contractions are seen in the distance to all of the C atoms 2 bonds away from the Fe center and in the multiple-scattering pathways with cooling of the sample.

2. XAS Pre-Edge Analysis. The analysis of the pre-edge region of $[Fe(\mathbf{PY5})(MeCN)]^{2+}$ and $[Fe(\mathbf{PY5})(Cl)]^{+}$ provides complementary information to the understanding of the electronic changes occurring in $[Fe(\mathbf{PY5})(N_3)]^{+}$ and [Fe-

---

(40) Sevillano, E.; Meuth, H.; Rehr, J. J. *Phys. Rev. B* **1979**, *20*, 4908−4911.

(41) Teo, B. K. *EXAFS: Basic Principles and Data Analysis*; Springer-Verlag: Boston, 1986.

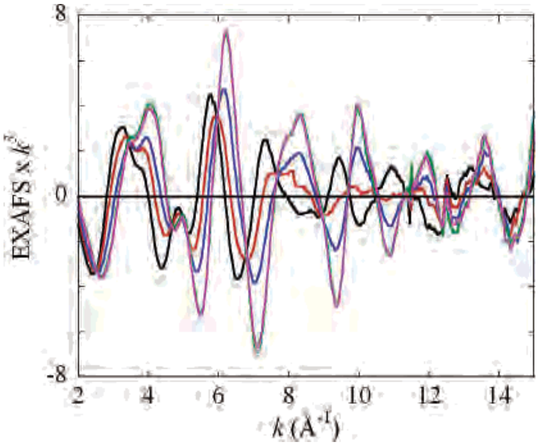

Figure 5. EXAFS data at RT (black), 150 K (red), 120 K (blue), 40 K (green), and 10 K (purple) for [Fe(**PY5**)(MeOH)]$^{2+}$, showing the geometric changes at the Fe site with cooling. The isosbestic behavior suggests variable fractions of LS and HS sites in each scan.

Table 5. EXAFS Fit Results for [Fe(**PY5**)(MeOH)]$^{2+}$ at RT and 10 K[a]

	R (Å)	σ^2 (Å^2)	ΔE_0	F[b]
		RT		
6 N/O[c]	2.13	0.0084	−9.45	0.069
12 C_2	3.09	0.0108		
10 N−C_2	3.37	0.0228		
10 N−C_3	4.51	0.0152		
5 N−C_4	4.66	0.0053		
		10 K		
6 N/O[c]	2.00	0.0039	−7.72	0.12
12 C_2	2.97	0.0072		
10 N−C_2	3.10	0.0154		
10 N−C_3	4.49	0.0169		
5 N−C_4	4.82	0.0050		

[a] Errors are estimated to be 0.01−0.03 Å for distances and 25% for coordination numbers. [b] Error (F) is defined as $F = \sum[[(\chi_{\mathrm{obsd}} - \chi_{\mathrm{calcd}})^2 k^6]/n]$, where n is the number of data points. [c] Backscatterers differing by ±1 atomic number (Z) are not distinguishable by EXAFS, here modeled as N.

(**PY5**)(MeOH)]$^{2+}$ as they undergo spin-crossover. Pre-edge fits to the spectrum of [Fe(**PY5**)(MeCN)]$^{2+}$ at RT and 10 K reveal 3 peaks at 7112.0, 7114.0, and 7116.5 eV. [Fe(**PY5**)(Cl)]$^{+}$ displays a low-intensity pre-edge with three peaks at 7111.4, 7112.3, and 7113.6 eV and a higher energy transition at 7115.4 eV at both RT and 10 K. The Fe K-edge spectra of [Fe(**PY5**)(MeCN)]$^{2+}$ and [Fe(**PY5**)(Cl)]$^{+}$ are given in Figure S9a, while [Fe(**PY5**)(MeCN)]$^{2+}$ is compared to two other LS complexes, [Fe(**PY5**)(CN)]$^{+}$ and [Fe(**PY5**)(pyridine)]$^{2+}$ (Figure S9b). [Fe(**PY5**)(X)]$^{n+}$ (X = MeCN, CN^{-}, pyridine) all have very similar spectra, with two transitions centered at ∼7112 and 7114 eV. Fits to the pre-edges of [Fe(**PY5**)(MeCN)]$^{2+}$ and [Fe(**PY5**)(Cl)]$^{+}$ at RT and 10 K are summarized in Table S1.

The fit to the pre-edge of RT [Fe(**PY5**)(N_3)]$^{+}$ (Table S1) is similar to that of HS [Fe(**PY5**)(Cl)]$^{+}$ (Figure 6). At 10 K, the spectrum has features consistent with a LS Fe^{II} **PY5** complex. Placing the [Fe(**PY5**)(N_3)]$^{+}$ sample at RT into the cryostat at 150 K and cooling the sample to 10 K over several hours, however, yielded a substantially different pre-edge spectrum and fits to the EXAFS data (not shown), changes that are currently under investigation.

The pre-edge and edge transitions of [Fe(**PY5**)(MeOH)]$^{2+}$ gradually change with decreasing temperature, consistent with the change for the EXAFS data (Figure 7). At RT, [Fe(**PY5**)(MeOH)]$^{2+}$ displays a pre-edge spectrum similar to that of [Fe(**PY5**)(Cl)]$^{+}$, suggesting a predominant HS configuration at RT. As the temperature is lowered, the pre-edge features slowly convert from those corresponding to a HS configuration to those corresponding to a LS configuration; the 10 K spectrum is similar to that of [Fe(**PY5**)(MeCN)]$^{2+}$ (Figure 8). As with the EXAFS data, the 150 and 120 K edge spectra can be simulated through summation of percentages of the RT and 10 K data, with resulting spectra that match the features of the observed data well (Figure S10). The edge data at 150 K predict a 40:60 LS:HS ratio; however, the pre-edge region is better simulated by a 30:70 ratio. The 120 K data are best simulated by a LS:HS configuration of 70:30 in both the edge and the pre-edge regions. These results are consistent with the simulations performed for the EXAFS region and with the solution magnetic susceptibility measurements.

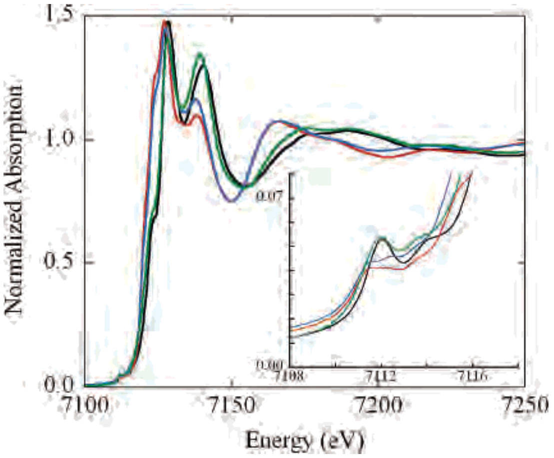

Figure 6. Fe K-edge data for [Fe(**PY5**)(MeCN)]$^{2+}$ at 10 K (black), [Fe(**PY5**)(Cl)]$^{+}$ at 10 K (red), [Fe(**PY5**)(N_3)]$^{+}$ at RT (blue), and [Fe(**PY5**)(N_3)]$^{+}$ at 10 K (green). The inset shows enlargement of the pre-edge (1s → 3d) transition area. The 10 K [Fe(**PY5**)(N_3)]$^{+}$ data are similar to the data of LS [Fe(**PY5**)(MeCN)]$^{2+}$, while the RT [Fe(**PY5**)(N_3)]$^{+}$ data are similar to HS [Fe(**PY5**)(Cl)]$^{+}$, which indicates that [Fe(**PY5**)(N_3)]$^{+}$ is undergoing a spin-transition as the temperature is lowered.

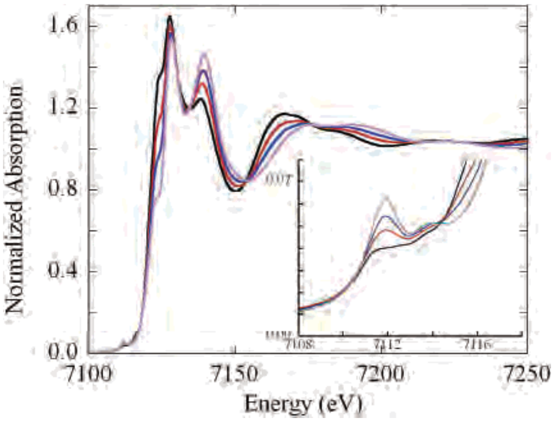

Figure 7. Fe K-edge data for [Fe(**PY5**)(MeOH)]$^{2+}$ at RT (black), 150 K (red), 120 K (blue), 40 K (green), and 10 K (purple). The inset shows enlargement of the pre-edge (1s → 3d) transition area. These edge data show the electronic changes at the Fe site as the complex undergoes the spin-transition with a decrease in temperature.

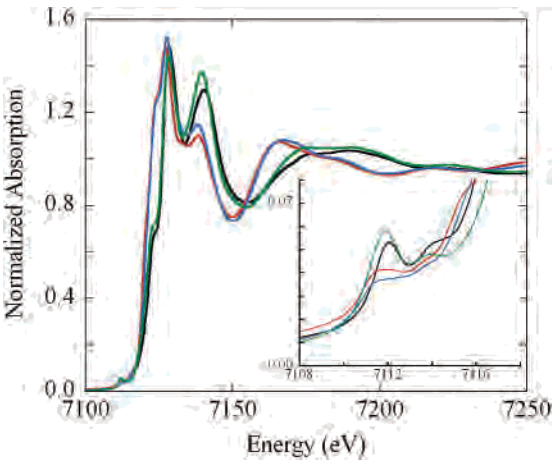

Figure 8. Fe K-edge data for [Fe(**PY5**)(MeCN)]$^{2+}$ at 10 K (black), [Fe(**PY5**)(Cl)]$^{+}$ at 10 K (red), [Fe(**PY5**)(MeOH)]$^{2+}$ at RT (blue), and [Fe(**PY5**)(MeOH)]$^{2+}$ at 10 K (green). The inset shows enlargement of the pre-edge (1s → 3d) transition area. The 10 K [Fe(**PY5**)(MeOH)]$^{2+}$ data are similar to the data of LS [Fe(**PY5**)(MeCN)]$^{2+}$, while the RT [Fe(**PY5**)(MeOH)]$^{2+}$ data are similar to HS [Fe(**PY5**)(Cl)]$^{+}$, which indicates that [Fe(**PY5**)(MeOH)]$^{2+}$ is undergoing a spin-transition as the temperature is lowered.

Discussion

In the study of bioinorganic chemistry, both low-spin (LS) and high-spin (HS) Fe^{II} and Fe^{III} species are encountered, often with similar coordination spheres. Due to the temperature-dependent spin-crossover heme systems identified by different spectroscopic techniques,[7−11] scientists using low-temperature spectroscopic techniques, such as electron paramagnetic resonance (EPR) and X-ray absorption spectroscopy (XAS), must use caution to ensure that the data collected accurately relate to the spin-state of the site. Our interest in modeling the reactivity of Fe-lipoxygenases led to the isolation of a series of Fe^{II} complexes: [Fe(**PY5**)(X)]$^{n+}$ (**PY5** = 2,6-bis(bis(2-pyridyl)methoxymethane)pyridine). The exogenous ligand, X, was shown to have a large influence on the electronic character of the Fe^{II} center at RT.[14] To fully gauge the electronic effect of the exogenous ligand in the series of [Fe(**PY5**)(X)]$^{n+}$ complexes, select compounds (X = MeCN, Cl$^-$, N$_3^-$, MeOH) were further investigated by a host of variable-temperature spectroscopic techniques. In particular, XAS has been used to characterize the electronic and structural changes that occur upon cooling.

While [Fe(**PY5**)(Cl)]$^{+}$ shows a slight counterion dependence in its solution magnetic susceptibility,[14,15] it exists in a HS configuration at all examined temperatures in both MeOH solution and the solid state. The results of the EXAFS and pre-edge analyses confirm this assignment. The fits to the EXAFS data at RT and 10 K are nearly identical, disregarding changes in σ^2 values due to thermal disorder, and analysis of the pre-edge region revealed typical HS octahedral Fe^{II} features.[20] Three peaks were necessary to fit the pre-edge data, and the intensities are similar to other HS ferrous octahedral complexes, such as [Fe(H$_2$O)$_6$]$^{2+}$.[20]

[Fe(**PY5**)(MeCN)]$^{2+}$ displays spectroscopic and metrical characteristics of a LS complex. Solution magnetic susceptibility measurements and a diamagnetic ^{1}H NMR spectrum indicate that the complex is LS at RT. EXAFS analyses corroborate this assignment. Analysis of the pre-edge region of the Fe K-edge spectrum of [Fe(**PY5**)(MeCN)]$^{2+}$ reveals a more complicated spectrum than anticipated for a six-coordinate LS ferrous complex. Typically, one peak in the 1s → 3d region is observed that is assigned as the transition to the unfilled e$_g$ set of the d manifold.[20] Occasionally, higher transitions (~3.5 eV above the 1s → 3d peak) are seen in the spectra of such complexes. These have been attributed to edge and not to 1s → 3d transitions.[20] The pre-edge region of [Fe(**PY5**)(MeCN)]$^{2+}$ is best fit with two peaks separated by ~2 eV, which is too large of an energy difference between the two empty e$_g$ orbitals to be accounted for by a distortion from an octahedral geometry. Comparison of the spectrum of [Fe(**PY5**)(MeCN)]$^{2+}$ with the spectra of LS [Fe(**PY5**)(pyridine)]$^{2+}$ and LS [Fe(**PY5**)(CN)]$^{+}$ indicates that these two peaks may be a signature for LS ferrous complexes employing the **PY5** ligand. Despite the atypical pre-edge spectrum of [Fe(**PY5**)(MeCN)]$^{2+}$, it is well characterized as a LS standard through magnetic susceptibility measurements and comparison to other LS [Fe(**PY5**)(X)]$^{n+}$ complexes.

Methanol and azide ligands have field strengths intermediate to those of acetonitrile and chloride ligands, leading to spin-crossover complexes. [Fe(**PY5**)(N$_3$)]$^{+}$ is able to undergo a spin-transition in MeOH with an inversion temperature of 207 K, the temperature at which a 50:50 LS:HS ratio exists. In the solid state, the inversion temperature is lowered to 156 K for crystalline samples. The SQUID data exhibit a gradual solution-like decrease in the $\chi_M T$ values with only a minor hysteresis in the higher temperature range (Figure 1). These data predict that at 135 K approximately 60% of the [Fe(**PY5**)(N$_3$)]$^{+}$ sites should exist in a LS configuration. This is in reasonable agreement with an 80% LS configuration estimate that can be determined from the average Fe−N distance of 2.046 Å of the 135 K structure, assuming an average Fe−N distance of 2.00 and 2.21 Å for pure LS and pure HS [Fe(**PY5**)(X)]$^{n+}$ complexes, respectively (Table 1). All attempts to model the crystallographic data as a binary mixture of LS and HS components, however, were unsuccessful. The XAS edge analyses of the RT and 10 K samples reveal predominant HS and LS components at RT and 10 K, respectively. Additionally, Fe−N distances reflecting the predominance of a HS complex at RT and a LS complex at 10 K were found through analysis of the EXAFS spectra.

[Fe(**PY5**)(MeOH)]$^{2+}$ exhibits spin-crossover behavior similar to that of [Fe(**PY5**)(N$_3$)]$^{+}$ with decreasing temperature both in solution and in the solid state. The XAS data on a finely ground solid reveal a gradual change as the temperature is decreased. The EXAFS and Fe K-edges display isosbestic points, indicating a two-component system, consistent with a predominantly HS site converting to a LS site upon cooling. Through simulations to the EXAFS and edge data, it is estimated that the sample is ~30−40% LS at 150 K and ~70% LS at 120 K, assuming that the spectra measured at RT and 10 K correspond to pure HS and LS complexes, respectively. The XAS edge spectra of [Fe(**PY5**)(MeOH)]$^{2+}$ change as the temperature is decreased, resembling the edge of [Fe(**PY5**)(Cl)]$^{+}$ at RT, while resembling the edge of [Fe(**PY5**)(MeCN)]$^{2+}$ at 10 K (HS to LS). While the XAS spectra show the slow conversion from a HS to a LS configuration as the temperature is lowered, the solid-state SQUID data display an abrupt cooperative transition at ∼90 K. Full spin-crossover to a LS configuration is never achieved, and the extent of this transition is highly variable depending upon the sample preparation. It is surprising that the XAS data, measured on a finely ground solid, are more consistent with the gradual change observed in the solution magnetic susceptibility data than with that in the solid-state data.

Summary

Structural and electronic investigations into the series of ferrous complexes, [Fe(**PY5**)(X)]$^{n+}$ (X = MeCN, Cl$^-$, N$_3^-$, MeOH), have been performed to provide insight into the changes that occur during temperature-induced spin-transitions. When X = MeCN, the complex remains LS at all temperatures. Conversely, when X = Cl$^-$, the complex is HS at all temperatures. Intermediate field-strength ligands (N$_3^-$, MeOH) allow the formation of spin-crossover complexes. [Fe(**PY5**)(N$_3$)]$^+$ undergoes a gradual spin-crossover from a HS to a LS configuration in the crystalline state by susceptibility measurements. The change in electronic configuration with cooling is also observable by XAS. In the case of [Fe(**PY5**)(MeOH)]$^{2+}$, isosbestic points in the XAS and EXAFS spectra reveal a neat and gradual transition from a predominantly HS to a predominantly LS distribution as the temperature is lowered. The SQUID data indicate an abrupt spin-transition, but full conversion to the LS configuration is never observed. It can therefore be stated that sample preparation plays a significant role in determining the specifics of the spin-transition in this complex.

This study provides an excellent lesson on the care that must be taken when preparing spin-transition complexes for analysis by different spectroscopic methods. Even minimal grinding of a crystalline sample can dramatically change the spin-transition behavior. Despite certain inconsistencies in the details of sample handling effects, these results provide the electronic and geometric basis for the direct characterization of spin-states in active sites of enzymes, as well as inorganic complexes.

Acknowledgment. We thank Prof. Jeffrey R. Long for the SQUID magnetometer data. Funding was provided by grants from the National Institutes of Health (GM50730 to T.D.P.S. and RR-01209 to K.O.H.) We are also grateful to the Stanford Graduate Fellowship Fund (C.R.G.) for financial support. XAS data were measured at SSRL that is supported by the Department of Energy, Office of Basic Energy Sciences. The Structural Molecular Biology program at SSRL is funded by the National Institutes of Health, National Center for Research Resources, Biomedical Technology Program, and the Department of Energy, Office of Biological and Environmental Research.

Supporting Information Available: Additional figures and crystallographic details. This material is available free of charge via the Internet at http://pubs.acs.org.

IC048765L